Research article

Guillermo Arregui, Martín F. Colombano, Jeremie Maire, Alessandro Pitanti, Néstor E. Capuj, Amadeu Griol, Alejandro Martínez, Clivia M. Sotomayor-Torres and Daniel Navarro-Urrios*

Injection locking in an optomechanical coherent phonon source

https://doi.org/10.1515/nanoph-2020-0592
Received November 2, 2020; accepted December 31, 2020; published online January 20, 2021

Abstract: Spontaneous locking of the phase of a coherent phonon source to an external reference is demonstrated in a deeply sideband-unresolved optomechanical system. The high-amplitude mechanical oscillations are driven by the anharmonic modulation of the radiation pressure force that result from an absorption-mediated free-carrier/temperature limit cycle, i.e., self-pulsing. Synchronization is observed when the pump laser driving the mechanical oscillator to a self-sustained state is modulated by a radiofrequency tone. We employ a pump-probe phonon detection scheme based on an independent optical cavity to observe only the mechanical oscillator dynamics. The lock range of the oscillation frequency, i.e., the Arnold tongue, is experimentally determined over a range of external reference strengths, evidencing the possibility to tune the oscillator frequency for a range up to 350 kHz. The stability of the coherent phonon source is evaluated via its phase noise, with a maximum achieved suppression of 44 dBc/Hz at 1 kHz offset for a 100 MHz mechanical resonator. Introducing a weak modulation in the excitation laser reveals as a further knob to trigger, control and stabilize the dynamical solutions of self-pulsing based optomechanical oscillators, thus enhancing their potential as acoustic wave sources in a single-layer silicon platform.

Keywords: injection locking; nonlinear dynamics; optomechanics; self-sustained oscillator.

***Corresponding author: Daniel Navarro-Urrios**, MIND-IN2UB, Departament d'Enginyeria Electrònica i Biomèdica, Facultat de Física, Universitat de Barcelona, Martí i Franquès 1, 08028 Barcelona, Spain, E-mail: dnavarro@ub.edu. https://orcid.org/0000-0001-9055-1583
Guillermo Arregui, Catalan Institute of Nanoscience and Nanotechnology (ICN2), CSIC and The Barcelona Institute of Science and Technology, Campus UAB, Bellaterra, 08193 Barcelona, Spain; and Dept. de Física, Universitat Autonoma de Barcelona, 08193 Bellaterra, Spain
Martín F. Colombano, Catalan Institute of Nanoscience and Nanotechnology (ICN2), CSIC and The Barcelona Institute of Science and Technology, Campus UAB, Bellaterra, 08193 Barcelona, Spain; and MIND-IN2UB, Departament d'Enginyeria Electrònica i Biomèdica, Facultat de Física, Universitat de Barcelona, Martí i Franquès 1, 08028 Barcelona, Spain
Jeremie Maire, Catalan Institute of Nanoscience and Nanotechnology (ICN2), CSIC and The Barcelona Institute of Science and Technology, Campus UAB, Bellaterra, 08193 Barcelona, Spain
Alessandro Pitanti, NEST Lab., CNR - Istituto di Nanoscienze and Scuola Normale Superiore, Piazza San Silvestro 12, 56217 Pisa, Italy
Néstor E. Capuj, Depto. Física, Universidad de La Laguna, 38200 San Cristóbal de La Laguna, Spain; and Instituto Universitario de Materiales y Nanotecnología, Universidad de La Laguna, 38071 Santa Cruz de Tenerife, Spain
Amadeu Griol and Alejandro Martínez, Nanophotonics Technology Center, Universitat Politècnica de Valencia, 46022 Valencia, Spain. https://orcid.org/0000-0001-5448-0140 (A. Martínez)
Clivia M. Sotomayor-Torres, Catalan Institute of Nanoscience and Nanotechnology (ICN2), CSIC and The Barcelona Institute of Science and Technology, Campus UAB, Bellaterra, 08193 Barcelona, Spain; and ICREA - Institució Catalana de Recerca i Estudis Avançats, 08010 Barcelona, Spain

Enabled by progress in nanofabrication, the enhanced coupling of optical and mechanical degrees of freedom in purposely engineered micro-/nanoscale structures has provided physicists with the possibility to observe new physical phenomena in both the classical and quantum regime [1]. In particular, their interaction in a mechanically compliant and laser-driven optical cavity has led to the design of cavity-optomechanical systems that enables both cooling [2] and amplification of mechanical motion [3] by mere selection of the driving laser wavelength. This versatility can be used for tasks spanning the exploration of the quantum nature of mesoscopic objects to on-chip signal processing. Among the applications are a new category of self-sustained radio-frequency oscillators called optomechanical oscillators (OMOs) [4] which, by construction, also serve as self-sustained coherent phonon sources and may be used as such. Since any physical property in a solid-state system depends on the exact positioning of the atoms, coherent acoustic phonons are extremely suited to dynamically manipulate electric [5, 6], optical [7, 8] and magnetic [9, 10] properties of matter.

Acoustic wave sources are therefore an enabling technology across physics as well as the first building block for information processing with phonons [11, 12].

Even though several strategies to induce mechanical lasing in optomechanical devices have been proposed [13, 14], OMOs based on a single optical and mechanical mode are probably the only practical small-footprint implementation [15, 16]. They can trigger an oscillation from a direct continuous source without needing feedback electronics using mechanisms such as the retarded radiation-pressure force [13], the back-action induced by the bolometric light force [17] or by coupling the optomechanical system to carrier/thermal self-sustained cyclic dynamics [18]. In these cases, their all-optical operation, ease of miniaturization, low power consumption and scalability make these oscillators potential candidates as optically driven phonon sources [19] and a possible replacement to conventional quartz-based oscillators in specific RF-photonic communication and sensing applications such as optical down conversion [20] or mass sensing [21]. Although the reported output stability of OMOs approaches state-of-the-art optoelectronic oscillators [22], their performance is often degraded by mechanical effects such as slow frequency drift [23], intrinsic [24] or thermomechanical noise [25] and by instabilities occurring at large displacement amplitudes [26]. Additional post-fabrication tunability of their phase and frequency as well as their noise characteristics are therefore critical for their improved performance as both acoustic wave sources and carriers in microwave photonics.

The behavior of a regenerative oscillator driven by an extra external oscillatory signal with a frequency close the oscillation frequency has been explored in a variety of systems such as lasers [27, 28] or masers [29], electrical tank circuits [30, 31], organ pipes [32], nonlinear mechanical resonators [33, 34], superconducting circuits [35] and human circadian rhythms [36]. These apparently dissimilar systems all share their tendency toward an adjustment of the oscillator's rhythm to the one externally imposed, as originally proposed by Adler [37]. In recent years, the intrinsic nonlinearity of the optomechanical interaction has been harnessed to explore the spontaneous locking of an oscillator to a reference signal delivered via the driving optical field [22, 38–40], via electrical capacitive actuation [41, 42] or by mechanical actuation with propagating acoustic waves [43]. In all these cases, the system is driven to a mechanical lasing state by dynamical back action, which requires a large optomechanical cooperativity [1]. In this article, we demonstrate spontaneous frequency locking of the coherent mechanical motion of a one-dimensional silicon optomechanical crystal (OMC) brought to a self-sustained state using the anharmonic modulation of the radiation pressure force due to the activation of a self-pulsing (SP) mechanism [44]. We use an independent optical cavity the radio-frequency spectrum of which is solely affected by the self-sustained mechanical dynamics. In this way, we overcome a drawback of the transduction schemes in previous power-modulated experiments, which often prevented an unambiguous assessment of the instantaneous amplitude of the mechanical oscillator due to the direct measurement of the reference oscillatory signal.

The particular system investigated here is a pair of close-by one-dimensional OMCs fabricated in a silicon-on-insulator wafer, as shown in the central SEM micrograph of Figure 1. We investigate the fundamental optical cavity mode of each OMC at wavelengths of 1531 nm (right-R) and 1550 nm (left-L), respectively, whose eigenfields are shown in Figure 1(c). Fabrication disorder distorts the nominal y-symmetry of the single OMC optical field profiles and naturally provides the spectral detuning between the two optical cavities, preventing any optical crosstalk as shown in the schematic of Figure 1. In addition, the same distortion leads to a high vacuum optomechanical coupling rate g_o between the optical resonances and the mechanical flexural modes with three antinodes along the x direction, that would otherwise be optomechanically dark. For the right OMC, this mechanical mode (Figure 1(b)) displays a frequency of f_R = 100.37 MHz and a calculated value of $g_{o,RR} = 2\pi \cdot 514$ kHz. The precise geometry and reasoning behind the clamping and interconnect structure has been described elsewhere [45], but it essentially allows the simultaneous optical excitation of the two optical modes as well as controlled phonon leakage from one beam to its neighbor. The mechanical eigenstructure of identical nanobeams would exhibit the symmetry of the system and would induce a perfect hybridization of the two mechanical modes into a symmetric and antisymmetric coupled modes. The mentioned fabrication disorder breaks the as-designed symmetry and the original string-like modes weakly hybridize as a result. However, the two-mode picture with in-phase and anti-phase oscillation still applies (see Supplementary Information). As a result of this weak coupling, a small part of the energy of the mechanical mode supported by the right beam (imperceptible in Figure 1(b)) resides in the left beam, which leads to a small calculated cross-coupling term of $g_{o,LR} = 2\pi \cdot 8$ kHz between the mechanical mode of the right OMC and the optical cavity of the left OMC, two orders of magnitude smaller than the direct term $g_{o,RR}$. The mechanical dynamics of the right OMC are controlled via a strong pump laser (dark blue in Figure 1) that couples light into the right optical cavity, eventually driving the mechanical mode into a free-running phonon lasing state at frequency $f_{\mathrm{OMO},0}$. In this coherent state, the mechanical dynamics are accessed by inspecting the optomechanical transduction of a weak probe optical signal (dark red in Figure 1) addressed on the left cavity, a signal that originates from the cross coupling term $g_{o,LR}$. When the pump laser is modulated with a weak RF tone at frequency f_{mod} far from the bare oscillation frequency $f_{\mathrm{OMO},0}$, this imprints an additional peak in the power spectral density (PSD) of the pump laser, but does not change the PSD of the probe laser, which, by construction, only shows the peak at f_{OMO}. Bringing f_{mod} sufficiently close to $f_{\mathrm{OMO},0}$ can lock the OMO to f_{mod}, which would lead to a single peak [38]. However, the direct spectral observation of the modulation imposed onto the pump when reading-out the pump after interaction with the sample complicates the unambiguous attribution of the presence of a single peak to injection locking at a particular modulation strength and frequency, as represented via the blue box in Figure 1. To discard the possibility that the external modulation is strong enough to quench the initially prepared lasing dynamical state, a direct determination of the mechanical dynamics is required. To this end the probe cavity is used. When the probe laser is analyzed at the output, the presence of a peak at $f_{\mathrm{mod}} = f_{\mathrm{OMO}}$ of similar magnitude to that observed at $f_{\mathrm{OMO},0}$ in the unlocked case is an unambiguous spectral evidence of injection locking, as depicted in the red box of Figure 1.

Measurements are performed at ambient conditions by bringing a tapered microloop optical fiber between the two structures, coupling light propagating in the fiber to the fundamental optical resonance of both beams (Figure 2(b)). The measured optical resonances have quality factors of $Q_R = 1.6 \cdot 10^4$ and $Q_L = 8.1 \cdot 10^3$, respectively, which are much lower than their calculated values $Q_{\mathrm{calc}} = 6 \cdot 10^5$ due to the presence of surface roughness. Simultaneous coupling to both cavities is achieved via two tunable near-infrared lasers (Yenista TUNICS T100S-HP) and an in-fiber combiner. The transmitted/reflected power is split and a Fabry–Pérot bandpass filter (BPF) in each arm is used to measure independently the light coming from the chosen laser, allowing the dynamics associated to both optical resonances to be read-out separately. The signals are fed to a spectrum analyzer (SPA), to a 5 GHz oscilloscope and/or to a vector network analyzer (VNA). The latter provides an AC voltage V_{AC} to an electro-optic modulator (EOM) and modulates the intensity of the input laser light, as well as measuring the magnitude and phase of the scattering response (S_{21}) of the system at the excitation frequency. The EOM is set at the quadrature point $V_{DC} = 0.5V_\pi$ to suppress higher harmonics, with the half-wave voltage given by $V_\pi = 6.7$ V. The full measurement setup is shown in Figure 2(a).

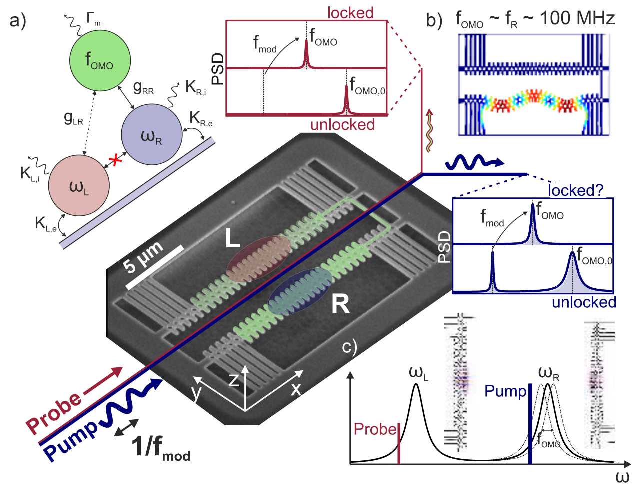

Figure 1: Optomechanical system and detection scheme. (a) Illustration of the optomechanical setting explored. Two optical cavities of frequencies ω_R (blue) and ω_L (red), with $\omega_R - \omega_L \gg \kappa_{L,R}$, can be driven via a common bus waveguide. A single mechanical mode of interest (green) is coupled optomechanically to both optical cavities, although the coupling strength is highly asymmetric, i.e., $g_{RR} \gg g_{LR}$. Cavity R is optically driven, leading to optomechanical self-oscillation of the mechanical mode at frequency $f_{\mathrm{OMO},0}$. This system is realized with two close-by silicon optomechanical crystal nanobeams that are connected by a mechanical link. Both beams support optical cavity modes that are spectrally and spatially isolated (c), as shown in the central SEM image. A flexural mode of the right beam (b) is selected by pumping (blue path) the right optical cavity mode at a wavelength and power where phonon lasing at frequency $f_{\mathrm{OMO},0} \sim f_m \sim 100$ MHz occurs. Due to the link, the mechanical mode also couples weakly to the left optical cavity, which is addressed via a probe optical signal (red path). The optomechanical transduction of the right (left) cavity exhibits a strong (weak) peak at the oscillation frequency $f_{\mathrm{OMO},0}$. If the pump laser is intensity-modulated at frequency f_{mod}, the PSD of transmitted pump (probe) light has (does not have) an additional peak at f_{mod}. Tuning f_{mod} can lead to injection locking. While the presence of a single peak is a necessary condition for injection locking, it is not a sufficient one in the pump PSD (blue box). The presence of a peak at f_{mod} in the PSD of the probe laser is however an unambiguous evidence of injection locking (red box).

Sweeping the laser (1) wavelength at high CW power from the blue-detuned side of the resonance at $\lambda_R = 1531$ nm to $\lambda = 1538$ nm leads to multiple dynamical states of the right OMC. For large detunings and relatively low intracavity photon numbers n_c, the incoherent mechanical motion activated by the thermal Langevin force imprints a modulation around the transmission DC value. The measured PSD is highlighted with dashed line 1 in the left colormap of Figure 2(c) and evidences the presence of several mechanical modes. In particular, the motion of the aforementioned mechanical mode at $f_R = 100.37$ MHz is transduced, with a measured natural linewidth of $\Gamma_m = 0.15$ MHz, i.e., $Q_m \sim 670$.

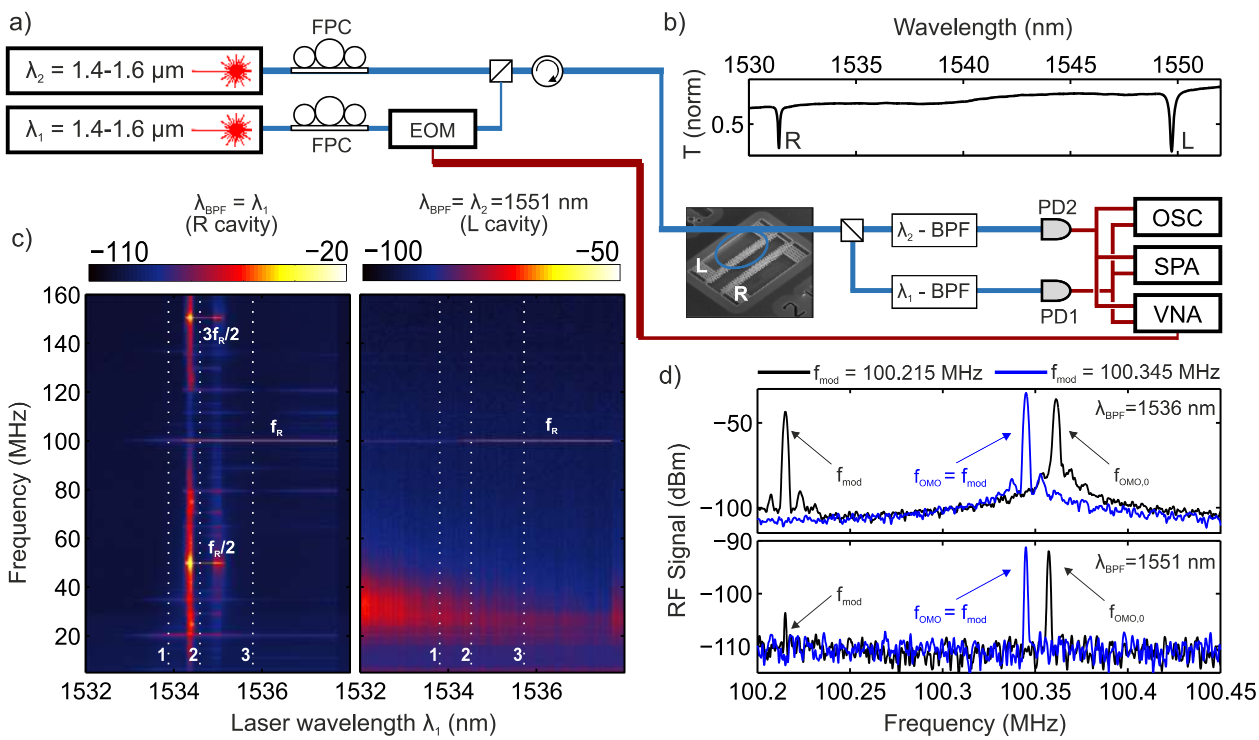

Figure 2: Experimental setup and device characterization.
(a) The main optical signals are derived from two external-cavity diode laser and sent into a tapered microloop optical fiber to evanescently couple light into the silicon optomechanical device. The optical signal from the OMC is collected by the same fiber taper and equally split in two, either in transmission or in reflection using an in-fiber circulator. The optical signals in both arms are band-pass filtered by narrow wavelength filters (λ-BPF) and impinge on two fast photodetectors (PDs). The electrical signals are sent to a spectrum analyzer (SPA), a vector network analyzer (VNA) or an oscilloscope (OSC) for characterization. EOM stands for electro-optic modulator and FPC for fiber polarization controller. (b) Optical transmission spectrum, exhibiting two optical modes at $\lambda_R = 1531$ nm and $\lambda_L = 1550$ nm. (c) Colormaps of the power spectral density (PSD) of the transmitted light when sweeping the laser (1) wavelength driving the optical resonance *R* at high power while another laser (2) weakly probes the resonance L; (left) $\lambda_{\mathrm{BPF}} = \lambda_1$ and (right) $\lambda_{\mathrm{BPF}} = \lambda_2$. The dashed white lines highlight (1) the thermal transduction, (2) $M = 2$ mechanical lasing and (3) $M = 1$ mechanical lasing states. (d) Within the configuration achieved in dashed line 3, adding a weak intensity-modulation via the EOM results in a peak in the PSD when its frequency f_{mod} is far from the phonon lasing frequency f_{OMO} (black signal), but locks the oscillator frequency for small detunings (blue signal). When the addressed signal is the probe, the spectra reproduce the ones schematically given in Figure 1.

As the wavelength, and therefore n_c, increases, the absorption in the tightly confined optical mode volume leads to the generation of free-carriers and to heating of the lattice. Since the refractive index of silicon depends on both temperature (ΔT) via the thermo-optic (TO) effect and free-carrier density (N_e) via free-carrier dispersion (FCD), so does the cavity wavelength. The cavity dynamics are therefore coupled to these two variables via the laser detuning, forming a system of nonlinear coupled differential equations with laser wavelength λ_L and power P_{in} as the free parameters. For particular values of these two, the system of equations exhibits a dynamical solution in the form of a anharmonic limit cycle, i.e. self-pulsing (SP), occurring at a frequency ν_{SP}. This results in a self-sustained oscillation of the cavity resonance around the laser line at a frequency ν_{SP} and coherently modulates the cavity photon number n_c. Since ν_{SP} depends on the driving parameters, further sweeping the wavelength tunes ν_{SP}. Whenever a harmonic of the SP approaches the mechanical frequency f_m, the photon number is modulated and the mechanical resonator is pumped via the radiation-pressure force $F_{rp} = \hbar G n_c$, with $G = g_o/x_{zpf}$. When this happens, the mechanical oscillation generally entrains the SP, forcing ν_{SP} to be a simple fraction M of f_m [46]. The system therefore undergoes self-sustained, coherent, high-amplitude mechanical oscillations, i.e., mechanical lasing. This can be observed for $M = 2$ and $M = 1$ in the white dashed lines 2 and 3 of Figure 2(c). Additional information on the SP and the induced phonon lasing is given in the Supplementary Information and elsewhere [18, 46]. The interest of using the neigboring OMC can be foreseen on the right colorplot of Figure 2(c), where the spectrum of laser (2) probing cavity L is shown as the wavelength of laser (1) is swept. They evidence that the amount of leaked mechanical energy coming from the oscillation of the right nanobeam and the resulting cross coupling term $g_{o,LR}$ enables reading the mechanical dynamics while filtering out other phenomena. Indeed, such a scheme disentangles the read-out of the mechanics from the cyclic dynamics of the free-carriers and temperature, the spatially diffusive nature and characteristic length-scales of which minimize their contribution to the neighbor cavity. It is observed that the modulation peak at 100.37 MHz is present for both an $M1$ and $M2$ phonon lasing states—dashed lines 2 and 3 in Figure 2(c)—without the presence of previous harmonics associated to the SP dynamics. The read-out laser (2) power is set to a value sufficiently high to transduce the incoming mechanical signal, but below its own SP Hopf bifurcation [47]. The broad spectral feature spanning 20–40 MHz across the right color-map of Figure 2(c) is a fingerprint of proximity to such bifurcation and is used as a sign of stability in the optical coupling conditions throughout the measurements. We therefore experimentally satisfy the detection scheme depicted in Figure 1, which opens the door to act upon the dynamical state of the complex self-pulsing/lasing state of the right cavity and observing the effect on the mechanical resonator dynamics via the left cavity. This experimental scheme was previously employed in the study by Colombano et al. [45], where both mechanical modes were brought to lasing and their motion synchronized. Further details are found in the Supplementary Information.

We focus now on the particular situation represented by dashed line 3 in Figure 2(c), where the right beam is pumped by laser (1) to the $M = 1$ mechanical lasing state at $f_{\mathrm{OMO},0} = 100.36$ MHz and we modulate the power of the laser at a frequency f_{mod} slightly detuned from the mechanical frequency ($V_{AC} = 0.004V_\pi$, $f_{\mathrm{mod}} = 100.215$ MHz). Note that the free-running self-sustained oscillation frequency $f_{\mathrm{OMO},0}$ in the absence of external modulation is usually smaller than the natural frequency f_R due to thermomechanical softening [48]. In the transmitted signal, RF spectrum two distinct peaks at the oscillator frequency $f_{\mathrm{OMO}} \sim f_{\mathrm{OMO},0}$ and at the modulation frequency f_{mod} are observed, as shown by the top black curve of Figure 2(d). For a smaller frequency difference, i.e., $f_{\mathrm{OMO},0} - f_{\mathrm{mod}} = 0.015$ MHz, only one peak at f_{mod} is observed (blue curve), which is a first fingerprint of injection locking [40]. However, this is unambiguously confirmed by employing the phonon detection scheme previously described. With the laser (2) as the probe set to be in resonance with the optical mode of the left beam and perfectly transmitted by the BPF, we are able to observe the mechanical lasing state of the neighbor cavity. When the modulation to laser (1) is on (bottom of Figure 2(d)), a peak at the modulation frequency f_{mod} becomes prominent only when the mechanical lasing is injection locked to the reference (blue curve) and $f_{OMO} = f_{mod}$. For a larger-frequency difference (black curve), only the transduction of the mechanical lasing at f_{OMO} is strong. Note that f_{OMO} in the bottom panel is slightly smaller than in the top panel due to temporal drift associated to thermal and/or alignment variations. In these modulation conditions, the presence of the small peak at the modulation frequency evidences the onset of nontrivial mechanical dynamics of the lasing cavity. Indeed, a possible contribution from free-carrier/temperature dynamics at f_{mod} has already been discarded by the fact that only the mechanical peak is detected in that configuration when the lasing cavity is in $M = 2$ (Figure 2(c)).

The range of modulation frequencies for which injection locking occurs, i.e., the Arnold tongue [49], is investigated by performing measurements such as those shown in Figure 2(d) while step-changing the excitation frequency from lower to higher frequencies. The results for $V_{AC} = 0.004V_\pi$, corresponding to a VNA tone of −5 dBm, are depicted as a color-map in Figure 3(a and b), with the BPFs centered in $\lambda = 1536$ nm and $\lambda = 1551$ nm, respectively. Note that during the acquisition of Figure 3(a and b), $f_{\mathrm{OMO}} = 100.322$ MHz in the absence of modulation is slightly lower than previously shown, which is due to a change in the optical coupling condition. Panel (a) clearly evidences the presence of an injection-locked region spanning 23 kHz, confirmed by the measurement performed on the other cavity (panel (b)). The absence of the directly transmitted and modulated light allows the evolution of the dynamics of the mechanical oscillator to be observed. The first remarkable observation is that prior to injection locking, the mechanical response exhibits a peak at the modulation frequency f_{mod}, indicating that the trajectory of the oscillator becomes non sinusoidal, as was already pointed out in Figure 2(d). Moreover, approaching the edges of the lock range, the peak at the mechanical lasing is dragged toward f_{mod}, i.e., frequency pulling [37, 50] occurs, which is a typical feature of self-sustained oscillators driven by an external source [22, 39]. At the borders of the lock range, the quasi-locked regime [38, 42], where the oscillator periodically oscillates between a locked and unlocked state [30], is observed (see Supplementary Information). In addition to acquiring the PSD signal of the transmitted light, the complex scattering parameter S_{21} of the system is measured by the VNA. Figure 3(c and d) shows its magnitude and phase when measured with the filter pass-band in resonance with either laser. The signal obtained by measuring at the pump laser wavelength is complex since both the modulation from the directly transmitted light and the modulation from the effect of the frequency tone on the cavity dynamics can interfere. However, the amplitude response observed in Figure 3(d) is simpler and shows that the oscillation amplitude of the mechanical oscillator remains constant throughout the lock range, at least for the corresponding modulation amplitude, and that the RF tone appearing at the borders outside that range follows the characteristic lineshape of a driven harmonic oscillator. Furthermore, the phase response $\Delta\phi$ is characterized by an evolution of approximately $\pi/2$ across the lock range, which is another standard feature of injection-locked electric tank oscillators [30] observed in power-modulated OMOs [38]. The PSD signal acquired for several modulation amplitudes V_{AC}, now only measuring with the filter transmitting the laser light outcoupled from the probe cavity, is depicted in Figure 4. This set of measurements clearly demonstrates the increasing size of the Arnold tongue with modulation amplitude and its asymmetric growth, i.e., a larger lock range at $f_{\mathrm{mod}} > f_{\mathrm{OMO,0}}$. This asymmetry, which is not reported in other injection-locked systems [38, 42], is simulated via numerical integration of the full system of equations (see Supplementary Information) and is not due to a hysteretic behavior of the system. It originates from high-order synchronization peaks [51] which are specially relevant here due to the specific anharmonic nature of the self-pulsing dynamics. For $V_{AC} > 0.007V_\pi$ the modulation at excitation frequencies f_{mod} close to $f_{\mathrm{OMO,0}}$ becomes too strong and the initial phonon lasing dynamics are lost, leading to a driven harmonic oscillator with a Lorentzian-like amplitude response in those regions and to an overall response that goes beyond pure locking.

As seen in Figure 4, injection locking controls the oscillation frequency over bandwidths as high as several hundreds of linewidths of the bare OMO. Locking to a low-noise reference also improves its stability, gauged over short times via its phase noise. The phase noise analysis was carried out with a different fiber taper, slightly changing the external coupling condition and resulting in an even wider Arnold tongue at a fixed modulation amplitude and exhibiting injection locking physics for voltages up to $V_{AC} = 0.015V_\pi$ ($P_{\mathrm{VNA}} = -10$ dBm). The phase noise measurements are carried

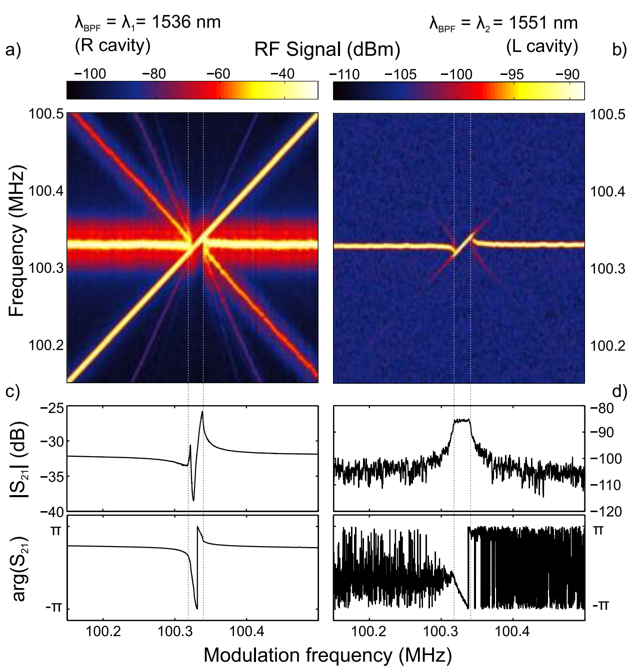

Figure 3: Spectral-domain evidence of injection locking to an external modulation.
(Color online) (a) Color plot of the power spectral density (PSD) of the transmitted light of the laser driving the right beam fundamental optical resonance at $\lambda_1 = 1536$ nm with $P_{\mathrm{in}} = 3$ mW when changing the modulation frequency in steps of 100 Hz. In a given range, the phonon lasing peak synchronizes to the modulation tone. (b) Equivalent measurement by observing light from the second laser that weakly probes the optical mode at $\lambda_2 = 1550$ nm of the left beam, allowing only the observation of the mechanical dynamics of the right beam. The coherent complex scattering response of the system measuring S_{21} in the VNA is depicted for the filter aligned with the laser driving the right (c) and the left (d) optical modes.

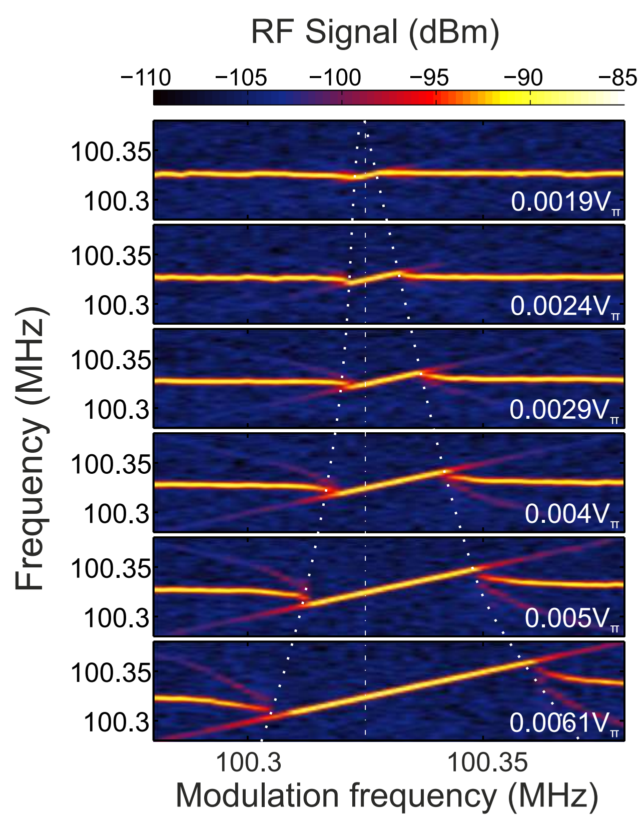

Figure 4: Phonon lasing oscillation frequency. (Color online) Colormaps of the power spectral density (PSD) of light transmitted at the wavelength of the probe laser for modulation amplitudes from $V_{AC} = 0.0019V_\pi$ to $V_{AC} = 0.0061\,V_\pi$. The dashed white lines are guides to the eye and help to visualize the asymmetric growth of the Arnold tongue with respect to the free-running oscillation frequency at $f_{\mathrm{OMO,0}} = 100.322$ MHz.

out using the dedicated module of the SPA and setting the frequency carrier to the oscillator frequency $f_{OMO,0}$, which matches f_{mod} inside the Arnold tongue. Figure 5(a) depicts the phase noise as a function of frequency offset for different levels of modulation power, starting from the free-running phonon lasing (black dashed line). We first see that for powers up to $P_{VNA} = -30$ dbm the phase noise increases for frequency offsets below 20 kHz. We attribute this to an unstable behavior of the system, giving rise to hopping between the locked and the unlocked state due to environmental noise. At larger excitation powers the OMO locks to the external reference and, from that modulation amplitude, a strong and progressive phase noise reduction can be observed, especially at frequency offsets below 30 kHz but spanning the full range of the phase noise measurement setup up to 1 MHz. The broad peak around 7 kHz arises from an unknown noise source in the optical path and is disregarded. The phase noise level at frequency offsets of 1, 10 and 100 kHz is given as a function of modulation amplitude in the inset to Figure 5. It shows both the increased low-offset phase noise prior to synchronization and an approximately linear phase noise reduction in the power lock range. A reduction of 1.1 dBc/Hz per excitation dBm is observed both at 1 kHz (blue) and 10 kHz (black), while the reduction is least pronounced at 100 kHz offset (red) and above. Given those values, the maximum achieved phase noise suppression is 44 dBc/Hz (1 kHz), 20 dBc/Hz (10 kHz) and 8.5 dBc/Hz (100 kHz). Last, the behavior of the phase noise at $P_{VNA} = -10$ dbm as a function of the modulation frequency f_{mod} across the full Arnold tongue is assessed. When the modulation tone is swept from 100 MHz, outside the lock range, the modulation tone appears as a noise peak at the frequency difference (see Figure 5(b)), as do all sidebands at frequency offsets $f = n|f_{OMO} - f_{mod}|$. Close to the onset of injection locking, at 100.22 MHz, where these additional peaks disappear, a considerable increase in the low-frequency offset phase noise is observed, that is also attributed to hopping between the locked and unlocked state [50]. This phase noise behavior is probably also associated to the quasi-locked regime described in the Supplementary Information. These considerations also apply in the opposite side of the lock range, where the increased phase noise is both more pronounced and extends throughout a broader range. Inside the Arnold tongue, the phase noise characteristics remain practically constant, evidencing the potential of injection locking to generate low-noise oscillatory references and coherent phonon sources with controlled frequency and purity.

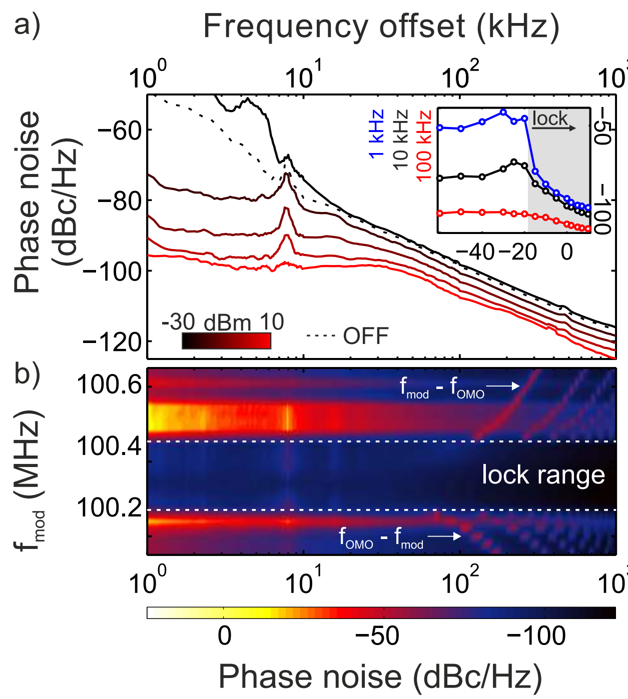

Figure 5: Phase noise characteristics.
(Color online) (a) Phase noise measurements of the phonon lasing state with a radio-frequency external tone at $f_{mod} \approx f_{OMO,0}$. The locked (unlocked) states are represented with black to red curves (dashed black line). The evolution of the phase noise at offsets 1, 10 and 100 kHz as a function of the modulation power P_{VNA} are depicted in the inset, with the lock power range in shaded gray. (b) Color plot of the phase noise as a function of the frequency offset for multiple driving frequencies f_{mod}. The chosen range for f_{mod} covers the full Arnold tongue for a drive power of $P_{VNA} = -10$ dbm.

In conclusion, we have reported the observation of injection locking of self-pulsing-driven regenerative oscillations of an optomechanical system to an external optical reference and isolated the mechanical signal by engineering the system geometry and read-out scheme. The lock range achieved can go up to 350 kHz, enabling a large tuning range over the oscillator frequency. Besides the direct consequences for acoustic wave self-sustained sources of the results shown here, applications using distributed arrays of oscillators within a single small-footprint chip, like robust time-keeping with standard optoelectronic oscillators [52], or neuromorphic computing [53], may benefit from the reported physics of injection locking from a variety of perspectives. Variations in natural mechanical frequencies due to unwanted fabrication variations make mutual synchronization of weakly coupled beams as in the study by Colombano et al. [45] relatively hard to observe. Due to the wide lock range achieved, injection locking can be used to presynchronize one of the coupled OMOs to an external drive and use it as a lead oscillator to which the others can synchronize via weak mechanical links, a configuration under exploration. Moreover, in cases where mechanical lasing of a particular mode cannot be achieved with an adiabatic laser parameter sweep, usually because the attained self-pulsing frequency ν_{SP} is still far from f_m, injection locking of the SP limit cycle to the external tone can be used to increase ν_{SP}. With this additional degree of freedom mechanical lasing can be reached, leading to a state that persists after the modulation is switched off, i.e., it enables exploration of usually inaccessible dynamical attractors of the system. Pulsed or modulated operation in this configuration could enable switching between different dynamical states, as reported in the study by Maire et al. [54] with a top pumping scheme. Furthermore, the feed forward nature of the technique stabilizes the oscillator without the need of feedback circuits, achieving a phase noise suppression up to 44 dBc/Hz at 1 kHz and 8.5 dBc/Hz at 100 kHz, resulting in an oscillator operated at atmospheric conditions with phase noise levels close to state of the art silicon optomechanical oscillators [16, 22, 55].

Acknowledgments: The authors thank Dr. E. Chavez for his careful and critical reading of the manuscript.

Author contributions: All the authors have accepted responsibility for the entire content of this submitted manuscript and approved submission.

Research funding: This research was funded by EU FET Open project PHENOMEN (GA: 713450). ICN2 is supported by the Severo Ochoa program from the Spanish Research Agency (AEI, grant no. SEV-2017-0706) and by the CERCA Programme/Generalitat de Catalunya. G. A. and C. M. S.-T. acknowledge the support from the Spanish MICINN project SIP (PGC2018-101743-B-I00). D. N. U., G. A. and M. F. C. gratefully acknowledge the support of a Ramón y Cajal postdoctoral fellowship (RYC-2014-15392), a BIST studentship, and a Severo Ochoa studentship, respectively. D. N. U. acknowledges the funding through the Ministry of Science, Innovation and Universities (PGC2018-094490-B-C22).

Conflict of interest statement: The authors declare no conflicts of interest regarding this article.

References

[1] M. Aspelmeyer, T. J. Kippenberg, and F. Marquardt, “Cavity optomechanics,” *Rev. Mod. Phys.*, vol. 86, p. 1391, 2014.

[2] J. Chan, T. P. M. Alegre, A. H. Safavi-Naeini, et al., “Laser cooling of a nanomechanical oscillator into its quantum ground state,” *Nature*, vol. 478, pp. 89–92, 2011.

[3] T. J. Kippenberg, H. Rokhsari, T. Carmon, A. Scherer, and K. J. Vahala, “Analysis of radiation-pressure induced mechanical oscillation of an optical microcavity,” *Phys. Rev. Lett.*, vol. 95, p. 033901, 2005.

[4] M. Hossein-Zadeh and K. J. Vahala, “An optomechanical oscillator on a silicon chip,” *IEEE J. Sel. Top. Quant. Electron.*, vol. 16, p. 276, 2010.

[5] E. Baldini, T. Palmieri, A. Dominguez, P. Ruello, A. Rubio, and M. Chergui, “*Phonon-driven selective Modulation of exciton oscillator Strengths in anatase TiO_2 Nanoparticles*,” *Nano Lett.*, vol. 18, p. 5007, 2018.

[6] A. Hernández-Mínguez, Y.-T. Liou, and P. V. Santos, “Interaction of surface acoustic waves with electronic excitations in graphene,” *J. Phys. D Appl. Phys.*, vol. 51, p. 383001, 2018.

[7] A. S. Kuznetsov, K. Biermann, and P. V. Santos, “Dynamic acousto-optical control of confined polariton condensates: from single traps to coupled lattices,” *Phys. Rev. Res.*, vol. 1, p. 023030, 2019.

[8] T. Czerniuk, C. Brüggemann, J. Tepper, et al., “Lasing from active optomechanical resonators,” *Nat. Commun.*, vol. 5, p. 4038, 2014.

[9] M. Weiler, H. Huebl, F. S. Goerg, F. D. Czeschka, R. Gross, and S. T. B. Goennenwein, “Spin pumping with coherent elastic waves,” *Phys. Rev. Lett.*, vol. 108, p. 176601, 2012.

[10] R. Mankowsky, A. von Hoegen, M. Först, and A. Cavalleri, “Ultrafast reversal of the ferroelectric polarization,” *Phys. Rev. Lett.*, vol. 118, p. 197601, 2017.

[11] K. Fang, M. H. Matheny, X. Luan, and O. Painter, “Optical transduction and routing of microwave phonons in cavity-optomechanical circuits,” *Nat. Photonics*, vol. 10, p. 489, 2016.

[12] W. Fu, Z. Shen, Y. Xu, et al., “Phononic integrated circuitry and spin-orbit interaction of phonons,” *Nat. Commun.*, vol. 10, p. 2743, 2019.

[13] T. Carmon, H. Rokhsari, L. Yang, T. J. Kippenberg, and K. J. Vahala, “Temporal behavior of radiation-pressure-induced vibrations of an optical microcavity phonon mode,” *Phys. Rev. Lett.*, vol. 94, p. 223902, 2005.

[14] I. S. Grudinin, H. Lee, O. Painter, and K. J. Vahala, “Phonon laser action in a tunable two-level system,” *Phys. Rev. Lett.*, vol. 104, p. 083901, 2010.

[15] I. Ghorbel, F. Swiadek, R. Zhu, et al., “Optomechanical gigahertz oscillator made of a two photon absorption free piezoelectric III/V semiconductor,” *APL Photonics*, vol. 4, p. 116103, 2019.

[16] L. Mercadé, L. L. Martín, A. Griol, D. Navarro-Urrios, and A. Martínez, “Microwave oscillator and frequency comb in a silicon optomechanical cavity with a full phononic bandgap,” *Nanophotonics*, vol. 9, p. 3535, 2020.

[17] C. Metzger, M. Ludwig, C. Neuenhahn, et al., “Self-induced oscillations in an optomechanical system driven by bolometric backaction,” *Phys. Rev. Lett.*, vol. 101, p. 133903, 2008.

[18] D. Navarro-Urrios, N. E. Capuj, J. Gomis-Bresco, et al., “A self-stabilized coherent phonon source driven by optical forces,” *Sci. Rep.*, vol. 5, p. 15733, 2015.

[19] D. Navarro-Urrios, J. Gomis-Bresco, F. Alzina, et al., “Self-sustained coherent phonon generation in optomechanical cavities,” *J. Opt.*, vol. 18, p. 094006, 2016.

[20] M. Hossein-Zadeh and K. J. Vahala, “Photonic RF down-converter based on optomechanical oscillation,” *IEEE Photonics Technol. Lett.*, vol. 20, no. 4, pp. 234–236, 2008.

[21] W. Yu, W. C. Jiang, Q. Lin, and T. Lu, "Cavity optomechanical spring sensing of single molecules," *Nat. Commun.*, vol. 7, p. 12311, 2016.
[22] X. Luan, Y. Huang, Y. Li, et al., "An integrated low phase noise radiation-pressure-driven optomechanical oscillator chipset," *Sci. Rep.*, vol. 4, p. 6842, 2014.
[23] A. B. Matsko, A. A. Savchenkov, and L. Maleki, "Stability of resonant opto-mechanical oscillators," *Opt. Express*, vol. 20, pp. 16234–16244, 2012.
[24] M. Sansa, E. Sage, E. C. Bullard, et al., "Frequency fluctuations in silicon nanoresonators," *Nat. Nanotechnol.*, vol. 11, pp. 552–558, 2016.
[25] C. M. Lin, T. T. Yen, V. V. Felmetsger, M. Hopcroft, J. H. Kuypers, and A. P. Pisano, "Thermally compensated aluminum nitride Lamb wave resonators for high temperature applications," *Appl. Phys. Lett.*, vol. 97, p. 083501, 2010.
[26] B. Yurke, D. S. Greywall, A. N. Pargellis, and P. A. Busch, "Theory of amplifier-noise evasion in an oscillator employing a nonlinear resonator," *Phys. Rev. A*, vol. 51, p. 4211, 1995.
[27] V. Annovazzi-Lodi, S. Donati, and M. Manna, "Chaos and locking in a semiconductor laser due to external injection," *IEEE J. Quant. Electron.*, vol. 30, p. 1537, 1994.
[28] Y. Liu, P. Davis, Y. Takiguchi, T. Aida, S. Saito, and J.-M. Liu, "Injection locking and synchronization of periodic and chaotic signals in semiconductor lasers," *IEEE J. Quant. Electron.*, vol. 39, p. 269, 2003.
[29] Y.-Y. Liu, J. Stehlik, M. J. Gullans, J. M. Taylor, and J. R. Petta, "Injection locking of a semiconductor double-quantum-dot micromaser," *Phys. Rev. A*, vol. 92, p. 053802, 2015.
[30] B. Razavi, "A study of injection locking and pulling in oscillators," *IEEE J. Solid State Circ.*, vol. 39, p. 1415, 2004.
[31] A. Mirzaei, M. E. Heidari, R. Bagheri, S. Chehrazi, and A. A. Abidi, "The quadrature LC oscillator: A complete portrait based on injection locking," *IEEE J. Solid State Circ.*, vol. 42, p. 1916, 2007.
[32] M. Abel, K. Ahnert, and S. Bergweiler, "Synchronization of sound sources," *Phys. Rev. Lett.*, vol. 103, p. 114301, 2009.
[33] M. J. Seitner, M. Abdi, A. Ridolfo, M. J. Hartmann, and E. M. Weig, "Parametric oscillation, frequency mixing, and injection locking of strongly coupled nanomechanical resonator modes," *Phys. Rev. Lett.*, vol. 118, p. 254301, 2017.
[34] D. Pu, R. Huan, and X. Wei, "Frequency stability improvement for piezoresistive micromechanical oscillators via synchronization," *AIP Adv.*, vol. 7, p. 035204, 2017.
[35] D. Marković, J. D. Pillet, E. Flurin, N. Roch, and B. Huard, "Injection locking and parametric locking in a superconducting circuit," *Phys. Rev. Appl.*, vol. 12, p. 024034, 2019.
[36] J. F. Duffy and C. A. Czeisler, "Effect of light on human circadian physiology," *Sleep Med. Clin.*, vol. 4, pp. 165–177, 2009.
[37] R. Adler, "A study of locking phenomena in oscillators," *Proc. IRE*, vol. 34, pp. 351–357, 1946.
[38] M. Hossein-Zadeh and K. J. Vahala, "Observation of injection locking in an optomechanical rf oscillator," *Appl. Phys. Lett.*, vol. 93, p. 191115, 2008.
[39] S. Y. Shah, M. Zhang, R. Rand, and M. Lipson, "Master-slave locking of optomechanical oscillators over a long distance," *Phys. Rev. Lett.*, vol. 114, p. 113602, 2015.
[40] K. Shlomi, D. Yuvaraj, I. Baskin, O. Suchoi, R. Winik, and E. Buks, "Synchronization in an optomechanical cavity," *Phys. Rev. E*, vol. 91, p. 032910, 2015.
[41] A. Pitanti, J. M. Fink, A. H. Safavi-Naeini, et al., "Strong opto-electro-mechanical coupling in a silicon photonic crystal cavity," *Opt. Express*, vol. 23, p. 3196, 2015.
[42] C. Bekker, R. Kalra, C. Baker, and W. P. Bowen, "Injection locking of an electro-optomechanical device," *Optica*, vol. 4, pp. 1196–1204, 2017.
[43] K. Huang and M. Hossein-Zadeh, "Injection locking of optomechanical oscillators via acoustic waves," *Opt. Express*, vol. 26, p. 8275, 2018.
[44] T. J. Johnson, M. Borselli, and Painter, "Self-induced optical modulation of the transmission through a high-Q silicon microdisk resonator," *Opt. Express*, vol. 14, p. 817, 2006.
[45] M. F. Colombano, G. Arregui, N. E. Capuj, et al., "Synchronization of optomechanical nanobeams by mechanical interaction," *Phys. Rev. Lett.*, vol. 123, p. 017402, 2019.
[46] D. Navarro-Urrios, N. E. Capuj, M. F. Colombano, et al., "Nonlinear dynamics and chaos in an optomechanical beam," *Nat. Commun.*, vol. 8, p. 14965, 2017.
[47] T. Van Vaerenbergh, M. Fiers, J. Dambre, and P. Bienstman, "Simplified description of self-pulsation and excitability by thermal and free-carrier effects in semiconductor microcavities," *Phys. Rev. A*, vol. 86, p. 063808, 2012.
[48] D. Navarro-Urrios, J. Gomis-Bresco, N. E. Capuj, et al., "Optical and mechanical mode tuning in an optomechanical crystal with light-induced thermal effects," *J. Appl. Phys.*, vol. 116, p. 093506, 2014.
[49] V. I. Arnold, *Geometrical Methods in the Theory of Ordinary Differential Equations*, 2nd ed. New York, Springer, 1988.
[50] A. Pikovsky, M. Rosenblum, and J. Kurths, *Synchronization: A Universal Concept in Nonlinear Sciences*, Cambridge, UK, Cambridge University Press, 2003.
[51] E. Amitai, N. Lörch, A. Nunnenkamp, S. Walter, and C. Bruder, "Synchronization of an optomechanical system to an external drive," *Phys. Rev. A*, vol. 95, p. 053858, 2017.
[52] X. S. Yao and L. Maleki, "Optoelectronic microwave oscillator," *J. Opt. Soc. Am. B*, vol. 13, p. 1725, 1996.
[53] F. C. Hoppensteadt and E. M. Izhikevich, "Synchronization of MEMS resonators and mechanical neurocomputing," *IEEE Trans. Circ. Syst. I, Reg. Pap.*, vol. 48, p. 133, 2001.
[54] J. Maire, G. Arregui, N. E. Capuj, et al., "Optical modulation of coherent phonon emission in optomechanical cavities," *APL Photonics*, vol. 3, p. 126102, 2018.
[55] J. Zheng, Y. Li, N. Goldberg, et al., "Feedback and harmonic locking of slot-type optomechanical oscillators to external low-noise reference clocks," *Appl. Phys. Lett.*, vol. 102, p. 141117, 2013.

Supplementary Material: The online version of this article offers supplementary material (https://doi.org/10.1515/nanoph-2020-0592).